Nanoscale

Accepted Manuscript

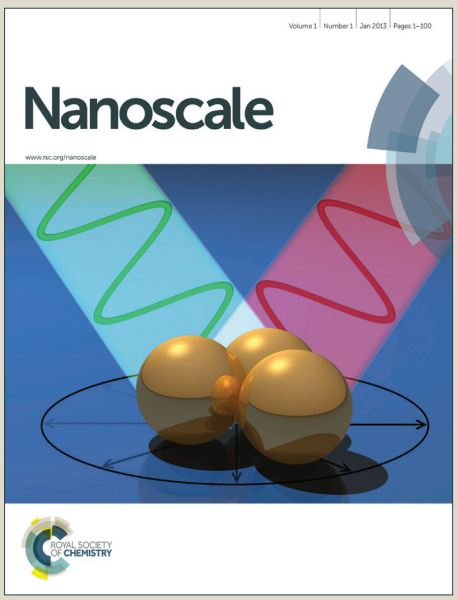

ROYAL SOCIETY OF CHEMISTRY

www.rsc.org/nanoscale

Journal Name

ARTICLE

Ultimate Conductivity Performance in Metallic Nanowire Networks

Received 00th January 20xx,
Accepted 00th January 20xx

DOI: 10.1039/x0xx00000x

www.rsc.org/

Claudia Gomes da Rocha[a,c,d]*, Hugh G. Manning[b,c,d], Colin O'Callaghan[a,c,d], Carlos Ritter[e], Allen T. Bellew[b,c,d], John J. Boland[b,c,d], and Mauro S. Ferreira[a,c,d]

In this work, we introduce a combined experimental and computational approach to describe the conductivity of metallic nanowire networks. Due to their highly disordered nature, these materials are typically described by simplified models in which network junctions control the overall conductivity. Here, we introduce a combined experimental and simulation approach that involves a wire-by-wire junction-by-junction simulation of an actual network. Rather than dealing with computer-generated networks, we use of a computational approach that captures the precise spatial distribution of wires from an SEM analysis of a real network. In this way, we fully account for all geometric aspects of the network, i.e. for the properties of the junctions and wire segments. Our model predicts characteristic junction resistances that are smaller than those found by earlier simplified models. The model outputs characteristic values that depend on the detailed connnectivty of the network, which can be used to compare the performance of different networks and to predict the optimum performance of any network and the scope for improvement.

Introduction

The unique behaviour displayed by nanoscale-sized materials is responsible for numerous scientific and technological breakthroughs. In comparison to their bulk counterparts, nanomaterials often reveal superior physical properties. Nonetheless, despite the unprecedented level of control that is currently possible over their structure, the manipulation of individual nanoscale components is still extremely laborious. For this reason, industry and academia have sought to exploit these functionalities without the need for precise nanomaterial placement. A candidate of particular interest is films comprised of randomly dispersed nanowires, commonly known as nanowire networks (NWNs).

NWNs are promising alternatives for a wide range of applications including flexible transparent conductors[1,2,3], thin-film solar cells[4], field effect phototransistor[5] and sensor[6] devices, to name but a few. Formed by randomly dispersed conducting wires, NWNs may function as conducting materials depending on the degree of connectivity of the network as well as on the quality of the junctions formed between neighbouring wires. Effective signal transmission through the wires depends on the nature of coating layers or surface functionalization on these wires. Because these coatings are typically dielectric in nature, NWNs can be thought of as an array of randomly dispersed conducting wires connected by capacitive junctions which will only conduct current if the voltage drop across a junction exceeds its characteristic threshold voltage[7]. Once this occurs, charge flows across the network through percolative paths formed by wires connected by resistive junctions.

The conduction properties of NWNs is dictated by a multitude of parameters such as the wire length and diameter distribution[8], interwire contact resistance, inner-wire resistance, wire density as well as their connectivity profile. With so many possible variables, such a study is best carried out through computer simulations. One way of simulating this percolative transport problem[9,10] is to map the network into a node voltage problem: each wire is represented by a circuit node at a common voltage connected to other wires by a certain number of junction resistances that depends on its connectivity within the network. Within this representation, it is then straightforward to obtain the overall conductance of a network by merely applying Ohm's and Kirchoff's current laws[11,12]. However, this approach involves an implicit assumption, hereafter referred to as the junction-dominated assumption (JDA), that the most significant contribution to the overall conductivity comes exclusively from the interwire junction resistances. This assumption is the basis for most

[a] School of Physics, Trinity College Dublin, Dublin 2, Ireland.
[b] School of Chemistry, Trinity College Dublin, Dublin 2, Ireland.
[c] Centre for Research on Adaptive Nanostructures and Nanodevices (CRANN), Trinity College Dublin, Dublin 2, Ireland.
[d] AMBER Research Centre, Trinity College Dublin, Dublin 2, Ireland.
[e] Departamento de Química, Universidade Federal do Paraná (UFPR), CP 19081, CEP 81531-990, Curitiba-PR, Brazil.

* gomesdac@tcd.ie

earlier descriptions of NWNs, including a recent theoretical calculation to describe the sheet resistance and the optical transmittance of Ag NWNs[13] where the characteristic junction resistance was then adjusted to match available experimental data[11].

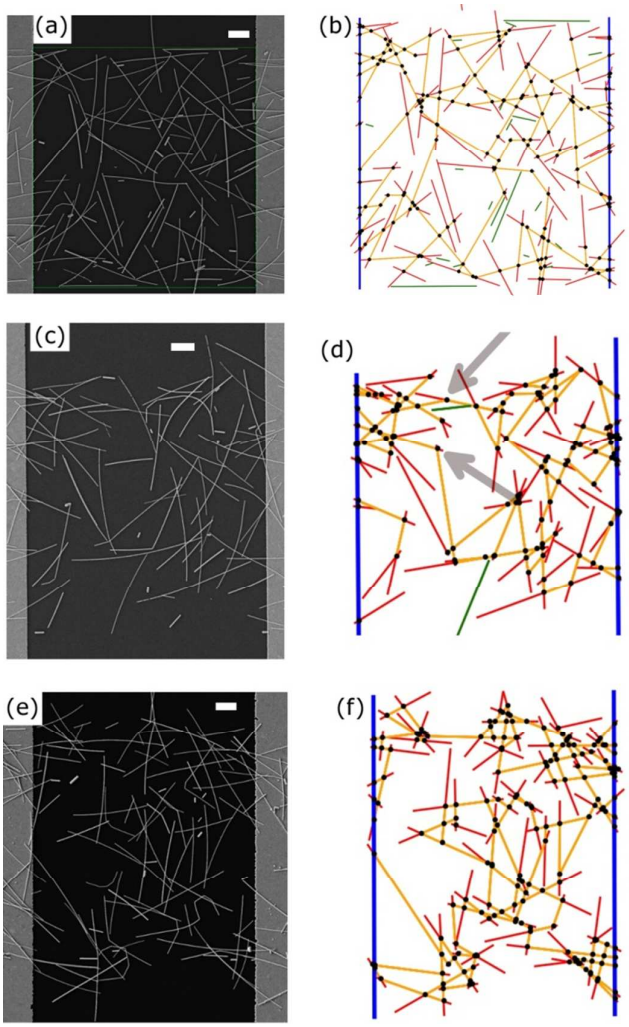

Figure 1: (Color online) (Left panels) Scanning electron micrograph (SEM) of silver nanowire networks containing densities of approximately (a) 0.28 and (c and e) 0.16 wires per μm^2. These networks are referred to in the text as #1, #2, and #3, respectively. Top scale bars represent 2 µm. (Right panels) Computational transcription of the networks shown on the left panels. Black dots mark the connections between wires represented by red sticks. Electrodes are represented by vertical blue sticks located on the extreme left and right of the figure. Isolated wires are represented by green sticks. Segments linking neighbouring connection points are highlighted in orange. Transparent grey arrows on panel (d) point at two critical junctions of the network.

The JDA is perfectly safe when the junction resistance is significantly larger than any other characteristic resistances within the network. This indeed is the case of NWNs comprised of carbon nanotubes[14,15]. However, the demands for increasingly conductive films, driven by efforts to reduce the junction resistances, will ultimately undermine the validity of the JDA due to its neglect of the inner resistances of the wires[16]. By relaxing the JDA, we can account not only for the geometric aspects of the network but also for the material properties of its components. Furthermore, by extending this picture to the limit of vanishingly small junction resistances we can provide an upper bound for the conductivity of the NWNs and reveal how much room there is to improve the conductivity of a film. Rather than working with computer-generated random networks, it is desirable to establish the upper bound for the conductivity of real networks. When conductivity measurements of such networks are compared with their respective upper bounds, one has a clear indication of how close to the optimum value they are. This calls for a computational tool capable of capturing the geometry of real networks combined with the ability to calculate the sheet resistance of the corresponding array of inter- and inner-wire resistors.

In this manuscript, in addition to relaxing the JDA as described above, we present for the first time a set of simulations that obtain the sheet resistance of networks with defined geometries through SEM image analysis of real samples (cf. Figure 1). In this way, we have a one-to-one correspondence between simulation and experiment and can simulate both the actual and ultimate network conductivity, the latter assuming the junction can be further optimized. Networks to be simulated were built from real experimental images of sparse and dense samples with wire densities (n) ranging from 0.15-0.6 wires per μm^2. This approach avoids the need for spatial configurational averaging highlighted in a recent paper in reference 12. Instead, our simulated network captures exactly the same spatial arrangement of the network displayed on the SEM images. The inner-wire resistance was included using a novel node-voltage approach capable of describing the transport properties of NWNs that also accounts for the wires resistivity. The model uses a new mapping scheme in which the wires of the network are described by a multi-nodal representation (MNR); the network topology is mapped as a graph carrying information about the wire junction connections and their respective separations. Critically, the model outputs for each network a set of characteristic values that are determined by the network connectivity and that allow comparisons between networks that are not possible using traditional configurational averaging based approaches.

Experimental and Computational methods

Experimental procedure

Ag nanowires (NWs) were purchased from Seashell Technology, LLC with an average length (diameter) of 6.7 µm (50 nm) (cf. supplemental information). Suitable single NWs were selected for contacting by electron beam lithography (EBL) after drop casting of NW/isopropanol dispersion (12.5 µg/ml) on clean Si substrates (1 µm thermal oxide) with pre-defined Ti/Au contact pads (5/25 nm). Isolated nanowire networks were formed by spray deposition of NW/isopropanol dispersion into EBL defined openings (120 µm x 20 µm) in bi-layer MMA (methyl methacrylate) and PMMA (poly methyl

methacrylate) e-beam resists. Post-spraying, wires on the resist were removed by acetone lift off; wires gathered into the openings formed the isolated nanowire networks. EBL was used to define contacts to single Ag NWs and isolated networks such that each item could be interrogated by four co-linear electrodes (cf. supplemental information). All contacts were metalized with Ag (120 nm).

Each section of the network bounded by adjacent electrodes was electrically stressed. Devices underwent electroforming by applying multiple 0 – 5 V dual sweeps stressing the network at increasing current compliance from the nA to mA range. The high current chosen ensures that the network conductivity is maximized with the vast majority of junction resistances optimized. This procedure has previously been shown to produce low resistance networks while avoiding potentially damaging high-temperature annealing steps[7,17]. Following this optimization step, a Kelvin (4-wire) resistance measurement was recorded. Current is sourced across the outer two electrodes and the drop in voltage is measured across the two innermost electrodes. This removes the contact resistance from the measurement and provides a true sheet resistance of the network. The resistivity for 15 single wire samples was also extracted using 4-probe resistance measurements. Wire diameters and channel lengths, including the electrodes' width[18] were measured using SEM (cf. supplemental material). All electrical measurements were carried out at ambient conditions using Keithley 4200 SCS. Imaging of nanowire networks was performed on a Zeiss Supra 40 SEM.

Simulations

Initially, we processed SEM images of 30 Ag NWN samples with distinct wire densities[19]. This was done by opening the image files on an interactive canvas widget that allowed us to characterize each NWN on a wire-by-wire basis. The data is converted into Cartesian coordinates that are subsequently used as inputs for solving the resistor network problem. Examples are depicted on Figure 1: micrograph images of real networks (left panels) are converted into mathematical objects (sticks) illustrated on the right panels. In instances of curved wires, we break the wire into smaller segments that approximately outline the wire curvature.

The standard way (JDA) of obtaining the transport characteristics of a given network containing N wires is to represent each wire by a node. The whole network is hence mapped into a voltage grid system of N nodes. Intersecting wires are represented by nearest-node neighbours connected by resistors that emulate active junctions (cf. Figure 2). Note that the spatial location of these nodes is irrelevant within JDA. From the connectivity profile of the network, one can build the resistance matrix ($\widehat{M}_R$) of the system as described in reference 12 and solve Kirchoff's circuit equation written in matrix form, $\widehat{M}_R\widehat{U} = \hat{I}$, where the vectors Û and Î are the potential at each wire and the current injected/drained out of the circuit, respectively[20]. The sheet resistance (R_s) is then obtained by evaluating $R_s = I / (U_L - U_R)$ where $U_{L(R)}$ is the potential on the left (right) electrode. The matrix $\widehat{M}_R$ carries the resistance values assigned to each interwire junction (R_j), which is assumed to be homogeneous throughout the network. It is worth pointing out that our main findings are not changed when we relax this assumption and allow R_j to follow a normal distribution. The role played by a normal dispersion on the junction resistance distributions can be found in the supplemental material[19].

The JDA scheme described above is attractive due to the ease of computational implementation. While it can provide an adequate qualitative interpretation about the conducting properties of networks, it lacks critical ingredients that must be taken into account. JDA description assumes that charge carriers hop ballistically from junction to junction without scattering by the wire material. As mentioned previously, this method fails whenever $R_j \approx R_{in}$, where R_{in} is the typical value for inner-wire resistance. Previous Monte Carlo simulations[21,22,23,24] on homogeneous networks above their percolation threshold have demonstrated that their transport properties are highly dependent on the ratio R_j/R_{in}. To move beyond JDA, we must introduce a new voltage-node mapping that is capable of including the inner-wire resistance.

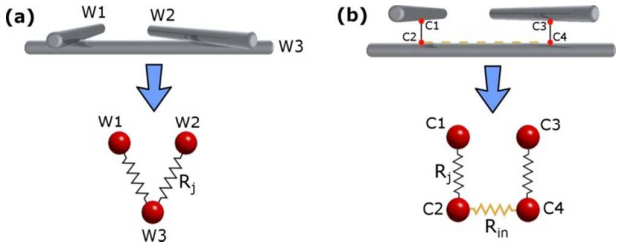

Figure 2: Nodal mapping schemes according to (a) JDA and (b) MNR models. JDA follows a wire-to-node criteria and the connection between nearest neighbor nodes are described by the junction resistance R_j. MNR accounts for R_j and inner wire resistances (R_{in}). This is done by mapping the connection points into nodes. Nearest neighbor nodes located in distinct wires are linked by junction resistances R_j whereas nearest neighbor nodes located on the same wire are linked by inner resistances R_{in}.

The resistance of an isolated wire is given by $R_{in} = \rho L/A_c$ where ρ is the wire resistivity, L its length and A_c the cross section area. In networks however, the wire resistance must be partitioned according to its number of intersections; a wire making k connections is partitioned into k+1 segments, each one of them carrying an inner resistance of $R_{in}^i = \rho\ell_i/A_c$ where i =1,..., k+1. Therefore, the novel voltage grid scheme must map the interwire connection points and not the wires, as done within JDA. This is illustrated in Figure 2; one can see that nodes are attributed to all connection points in all wires. This gives a total number of nodes of $2N_c$ where N_c is the number of interwire connections of the network. This new mapping scheme generates a network that is topologically different from JDA and will be referred to as multi-nodal representation (MNR) since the wires can be described by multiple nodes. Note that in this scheme, the position of the nodes matters. If two nodes share the same set of (x,y) coordinates, they characterize an interwire connection with junction resistance R_j. If two nodes belong to the same wire and are nearest neighbours, they feature an inner-wire

segment which consequently has a resistance associated to it. Note also that the computational implementation of our approach does not require the use of 3D objects (e.g. cylinders)[25] in order to account for the wire thickness. The networks can be still described by sticks dispersed on a plane since the diameter of wires is incorporated in the inner-wire resistances.

The determination of nearest nodes is done by viewing the whole network as a graph composed of vertices (junction points) and edges (wire segments). An adapted breadth-first search[26] algorithm was implemented to inspect the whole network - represented as a graph - and to determine its complete chart of neighbouring node pairs. In this way, one can construct a new resistance matrix $\widehat{M}_R$[20] which is plugged into Kirchoff's circuit law to obtain the sheet resistance of the samples. Results obtained via both models (JDA and MNR) are compared in the following section.

Discussion and results

To implement MNR, we used a resistivity value of ρ = 22.6 ± 2.3 nΩm determined from room temperature resistance measurements of a distribution of 15 Ag nanowires with diameters of D = 50 ± 13 nm based on a SEM analysis of 101 Ag NWs[19]. It is important to note that surface scattering effects

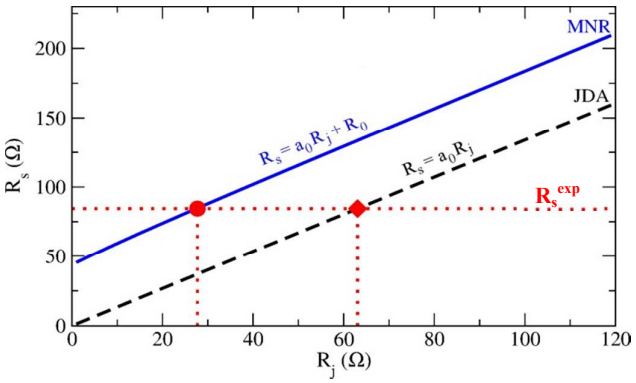

Figure 3: (Color online) Sheet resistance (R_s) versus junction resistance (R_j) analysis performed on sample #1 using JDA (black dashed line) and MNR (blue solid line) models. Horizontal dotted line (red) marks the measured sheet resistance value (R_s^{exp} = 84.42 Ω). Circle and diamond dots indicate the estimated junction resistance within MNR and JDA, respectively. Fitting line expressions used to obtain a_0 and R_0 values are added on top of each numerical curve.

will depend on wire diameter and temperature[27] so that wire resistance measurements must be performed on representative wires and under the appropriate temperature conditions before this model can be applied more generally. These values were employed in all 30 NWN samples mapped from micrograph images. Figure 3 shows the results obtained when JDA and MNR methods are applied on network #1 shown in Fig. 1a and b. This sample exhibits wire density of n = 0.28 μm^{-2} and a measured sheet resistance of R_s^{exp} = 84.42 Ω. The sheet resistance calculated as a function of the junction resistance R_j is plotted for JDA (black dashed line) and MNR (blue solid line). The horizontal dotted line corresponds to R_s^{exp}. As expected, the sheet resistance grows linearly with R_j for both descriptions (JDA and MNR). The models however differ in specific ways: JDA predicts that $R_s = a_0 R_j$, whereas MNR finds $R_s = a_0 R_j + R_0$, where a_0 is the slope and R_0 is the resistance that the network would have if all interwire contacts were perfect. Thus the R_0 shift between JDA and MNR models accounts for the influence of the inner-wire resistance on the overall sheet resistance and it is purely determined by the network geometry and its detailed connectivity. One immediate consequence of this shift is that the JDA tends to overestimate the junction resistances. The diamond and the circle on Figure 3 identify the value of R_j^{exp} in the JDA and MNR respectively that corresponds to the measured sheet resistance R_s^{exp}. The JDA-estimate for R_j^{exp} is found to be approximately 40 Ω higher than for the MNR for this particular sample, and R_0 = 46.43 Ω. With such a large contribution from the resistance of the network skeleton, it is not surprising that R_j is overestimated by the same order of magnitude. In fact, recent attempts to obtain the junction resistances of NWNs within JDA have reported values of the order of 2 kΩ, which is substantially larger than the values measured across individual junctions[11]. The risk of an overestimation in R_j is that it might raise false hopes that the junctions of a network can be further

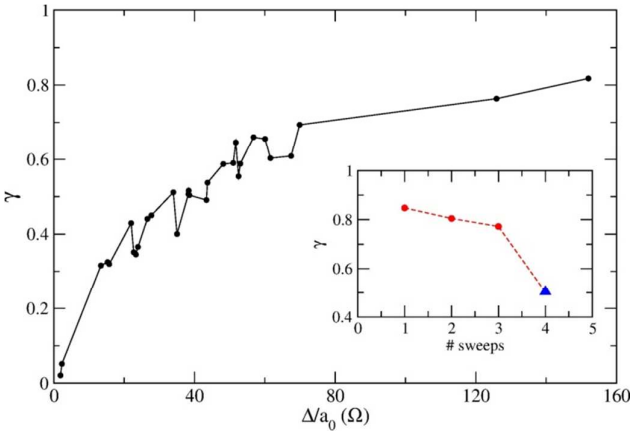

Figure 4: Optimization-capacity coefficient (γ) versus estimated characteristic junction resistance (Δ/a_0) for all 30 networks studied in this work. Inset: γ values obtained at four voltage sweep steps applied on sample #30 (cf. Table S1[19]). The triangle corresponds to its saturation state with a measured sheet resistance of R_s^{exp} = 76.68 Ω.

optimized. Once again, it is worth reiterating that the JDA model is only valid when the transport is dominated by junction resistances, i.e. when $R_s^{exp} >> R_0$ and so the inclusion of the inner-wire resistance contributions will cause minor changes to the estimated values of R_j.

Another interesting consequence of relaxing the JDA is that by defining a quantity $\Delta = R_s^{exp} - R_0$, we can estimate how close (or far) a particular sample is from operating at its minimum resistance state R_0. For this particular sample Δ = 37.99 Ω, which means that the sheet resistance is about 38 Ω above its minimum resistance state. A more descriptive quantity that establishes how much room for improvement a network has is given by $\gamma = 1 - R_0/R_s^{exp}$. This dimensionless quantity, named optimization-capacity coefficient, ranges from 0 to 1. Values of γ close to 1 represent networks whose conductivities can be

considerably improved since their sheet resistances are far from the optimal value R_0. When γ approaches 0, on the other hand, the network is close to its optimum conductivity and is unlikely that it can be further optimized. The ability to establish how much potential for optimization a network has serves as a useful guide in the search for networks with continuously larger conductivity values.

The characteristic values outputted by the model allow us to compare different networks. Table 1 shows the γ values for the three networks that are discussed in detail here, together with the corresponding values of n, R_0, R_s^{exp}, Δ, and Δ/a_0 (R_j^{exp}) obtained within MNR. We note $\Delta/a_0 = R_j^{exp}$ since $R_s^{exp} = a_0 R_j^{exp} + R_0$. The complete table containing the characteristic values for all 30 samples can be found in the supplemental information. No obvious correlation is seen between the optimization-capacity coefficient and either of these quantities, suggesting that γ may contain a rather non-trivial dependence. However, when γ is compared against the ratio Δ/a_0 for all 30 networks, a clear trend is observed. As shown in Figure 4, a plot of γ as a function of Δ/a_0 displays a monotonic behaviour that spans the entire range of possible values for the optimization-capacity coefficient which is not very surprising given Δ/a_0 can be thought of as the estimated characteristic junction resistance. In spite of that, the fact that the diverse range of networks in table S1[19] falls onto such a smooth curve suggests a very robust, if not universal, trend that is likely to be followed by all networks.

Besides determining the optimization-capacity coefficient for different networks, this quantity can also be used to assess how one specific network evolves as it is electrically stressed. Consecutive voltage sweeps are known to increase the conductivity of the network from completely inactive all the way to its fully optimized state. The quantity R_0 is determined by the geometry of the network (and will not change with the consecutive voltage sweeps) but the measured values of R_s^{exp} change as the network is stressed. The inset of Figure 4 shows γ after a sequence of voltage sweeps. Note that it starts with a relatively large value of γ but it decays continuously indicating that the network is evolving towards its optimum value. Once again, γ appears as a useful quantity that can be employed to assess how much room there is to increase the conductivity of the NWNs.

Comparisons between networks

To highlight the advantage of using image processing techniques to reproduce the exact spatial distribution of real networks, we have selected to discuss the peculiar case of two samples shown in Fig. 1c-f that exhibit very distinct characteristic values (Δ/a_0, R_0, and γ) but rather similar sheet resistances and same wire density (0.16 wires per μm^2). In this example, the simple intuitive relationship between density and sheet resistance fails to account for the critical role of connectivity in the performance of sparse films. The characteristic values within our model capture differences in connectivity for networks of similar densities. To demonstrate this, we present the image analysis of two samples labelled here as #2 and #3 (cf. Fig. 1c-f) and their characteristic values can be found on Table 1. Although both samples have the same wire density, their connectivity profiles differ remarkably. Sample #2 has fewer paths connecting one electrode to another compared with sample #3. Therefore, the distinct characteristic Δ/a_0, R_0, and γ values of each sample carry information about the inherent features of the networks that are hidden when analyzing global quantities such as sheet resistance versus density trends. An analysis of Figure 1d reveals that the performance of network #2 relies basically on 2 junctions identified by the gray arrows. Those junctions are the main bridges connecting the electrodes. Since all the networks are mapped as a graph, we can quantify their importance by calculating their betweenness centrality[28] degree. This critical property quantifies the number of times a node must be visited to connect the shortest path between two other nodes. Those two junctions are the ones with the highest betweenness levels and they play a major impact on the current propagation across the network. Critically, this kind of information can only be accessed via our approach where the network is mapped wire-by-wire, junction-by-junction. This method turns out to be extremely important for sparse networks such as samples #2 and #3 where each wire and each junction makes an important contribution to the conductivity.

Conclusions

We have introduced a novel computational method that exactly reproduces the spatial arrangement of experimentally generated NWNs through image analysis, so as to include the contribution of the inner-wire resistance in the calculation of the conductivity of these materials. Often neglected when the conductivity is dominated by junction resistances, the inner-wire resistances may play a significant role in the overall conductivity of NWNs. When the inner-wire resistances are neglected, results for the junction resistance tend to be overestimated. Regarding the prospects for optimization of the network conductivity, it is important to have a realistic estimate of the quality of the junctions. If junction resistances are small (large), it is unlikely (likely) that they can be further improved. It is thus essential to be able to estimate them accurately. Furthermore, by including the inner-wire resistance contribution in our calculations we can establish an upper bound for the conductivity of NWNs by simply imposing ideal lossless junctions. A simple comparison of measured values of sheet resistances with the corresponding optimum values can tell how realistic the chances of further improving the network conductivity are. Rather than providing a qualitative assessment of the chances for improvement, we quantify the ease of improvement by introducing the optimization-capacity coefficient γ. This allows us to compare between different networks, identifying those which can be further improved. Similar analysis can be used to study the evolution of one specific network as it is electrically stressed. Our model explicitly avoids the use of configurational averaging over the spatial distribution of wires in computer-generated networks, which is known to cause significant fluctuations in the

calculated values of sheet resistance especially in the case of sparse samples. It also provides unique insights about the networks´ connectivity. Networks with similar wire densities and sheet resistances may have rather distinct connectivity profiles which are imprinted on the characteristic values determined within our model, providing insights that are simply not accessible using conventional configurational averaging approaches.

Table 1: Wire densities (n), and characteristic junction resistances (Δ/a_0) of all Ag NWN samples obtained by fitting the measured sheet resistance (R_s^{exp}) with the calculated curves R_s vs. R_j derived within MNR. Values of Δ, R_0 as well as γ are also depicted.

Network	n (NW/ μm^2)	γ	Δ (Ω)	Δ/a_0 (Ω)	R_0 (Ω)	R_s^{exp} (Ω)
#1	0.28	0.45	37.99	27.73	46.43	84.42
#2	0.16	0.42	67.43	27.52	92.05	159.95
#3	0.16	0.65	116.15	60.07	60.99	177.14

Acknowledgements

The authors wish to acknowledge funding from the European Research Council (ERC) under Advanced Grant 321160. This publication has emanated from research supported in part by a research grant from Science Foundation Ireland (SFI) under Grant Number SFI/12/RC/2278. C. R. wishes to acknowledge the Brazilian National Council for Scientific and Technological Development (CNPq). The support of TCHPC at Trinity College Dublin for computational resources is also acknowledged. C. G. R., C. O'C., and C. R. developed the new modelling scheme and performed all simulations; H. M. carried out the experiments on Ag NWNs and A. T. B. performed experiments on individual NWs junctions; J. J. B. led the experimental effort and M. S. F. guided the simulation team and led the overall research.

Notes and references

‡ Footnotes relating to the main text should appear here. These might include comments relevant to but not central to the matter under discussion, limited experimental and spectral data, and crystallographic data.
§
§§
etc.

1 A. Kumar, Z. Zhou, ACS Nano 2010, **4**, 11.
2 S. De, T. M. Higgins, P. E. Lyons, E. M. Doherty, P. N. Nirmalraj, W. J. Blau, J. J. Boland, J. N. Coleman, ACS Nano 2009, **3**, 1767.
3 S. De, J. N. Coleman, MRS Bull. 2011, **36**, 774.
4 S. Xie, Z. Ouyang, B. Jia, M. Gu, Opt. Express 2013, **21**, A355.
5 B.-R. Huang, J.-F. Hsu, C.-S. Huang, Y.-T. Shih, K.-S. Lu, Mat. Sci. Eng. C 2007, **27**, 1197.
6 B. Y. Lee, M. G. Sung, H. Lee, S. Namgung, S. Y. Park, D. S. Choi, S. Hong, NPG Asia Mater. 2010, **2**, 103.
7 P. N. Nirmalraj, A. T. Bellew, A. P. Bell, J. A. Fairfield, E. K. McCarthy, C. O'Kelly, L. F. C. Pereira, S. Sorel, D. Morosan, J. N. Coleman, M. S. Ferreira, J. J. Boland, Nano Lett. 2012, **12**, 5966.
8 S. Sorel, P. E. Lyons, S. De, J. C. Dickerson, J. N. Coleman, Nanotechnology 2012, **23**, (18), 185201.
9 S. Kirkpatrick, Rev. Mod. Phys. 1973, **45**, 574.
10 I. Balberg, N. Binenbaum, C. H. Anderson, Phys. Rev. Lett. 1983, **51**, 1605.
11 R. M. Mutiso, M. C. Sherrott, A. R. Rathmell, B. J. Wiley, K. I. Winey, ACS Nano 2013, **7**, 7654.
12 J. A. Fairfield, C. Ritter, A. T. Bellew, E. K. McCarthy, M. S. Ferreira, J. J. Boland, ACS Nano 2014, **8**, 9542.
13 S. De , P. J. King , P. E. Lyons , U. Khan , J. N. Coleman, ACS Nano 2010, **4**, 7064.
14 P. N. Nirmalraj, P. E. Lyons, S. De, J. N. Coleman, J. J. Boland, Nano Lett. 2009, **9**, 3890.
15 D. Hecht, L. Hu, G. Grüner, App. Phys. Lett. 2006, **89**, 133112.
16 A. T. Bellew, A. P. Bell, E. K. McCarthy, J. A. Fairfield, J. J. Boland, Nanoscale 2014, **6**, 9632. Results for individual junction resistances measured in Ag nanowires are to be submitted.
17 T.-B. Song, Y. Chen, C.-H. Chung, Y. Yang, B. Bob, H.-S. Duan, G. Li, K.-N. Tu, Y. Huang, Y. Yang, ACS Nano 2014, **8**, 2804.
18 M. M. Koleśnik, S. Hansel, T. Lutz, N. Kinahan, M. Boese, V. Krstić, Small, 2011, **7**, 2873.
19 Supplemental Material.
20 C. Pozrikidis, "An Introduction to Grids, Graphs, and Networks", OUP USA (17 April 2014).
21 J. Li, S.-L. Zhang, Phys. Rev. E 2009, **80**, 040104(R); Phys. Rev. E 2010, **81**, 021120.
22 J. Hicks, A. Behnam, A. Ural, Phys. Rev. E 2009, **79**, 012102.
23 M. Žeželj, I. Stanković, Phys. Rev. B 2012, **86**, 134202.
24 M. Žeželj, I. Stanković, A. Belić, Phys. Rev. E 2012, **85**, 021101.
25 S. I. White, B. A. DiDonna, M. Mu, T. C. Lubensky, K. I. Winey, Phys. Rev. B 2009, **79**, 024301.
26 Skiena, Steven (2008). The Algorithm Design Manual. Springer. p. 480. DOI:10.1007/978-1-84800-070-4_4.
27 A. Bid, A. Bora, A. K. Raychaudhuri, Phys. Rev. B 2006, **74**, 035426.
28 U. Brandes, Soc. Networks 2008, **30**, 136.